Optical guiding of absorbing nanoclusters in air

Vladlen G. Shvedov[1−3], Anton S. Desyatnikov[1*], Andrei V. Rode[3], Wieslaw Krolikowski[3], and Yuri S. Kivshar[1]

[1]*Nonlinear Physics Center, Research School of Physics and Engineering, The Australian National University, Canberra ACT 0200, Australia*
[2]*Department of Physics, Taurida National University, Simferopol 95007 Crimea, Ukraine*
[3]*Laser Physics Center, Research School of Physics and Engineering, The Australian National University, Canberra ACT 0200, Australia*

asd124@rsphysse.anu.edu.au

Abstract: We suggest a novel approach in all-optical trapping employing a photophoretic force for manipulation of absorbing particles in open air. We demonstrate experimentally the robust three-dimensional guiding, over the distances of a few millimeters, of agglomerates of carbon nanoparticles with the size spanned from 100 nm to 10 μm, as well as their acceleration up to velocities of 1 cm/sec. We achieve stable positioning and guiding of particles as well as simultaneous trapping of a large number of particles in a dual beam optical trap created by two counter-propagating and co-rotating optical vortex beams.

OCIS codes: (350.4855) Optical tweezers or optical manipulation; (260.6042) Singular optics; (160.4236) Nanomaterials

References and links

1. A. Ashkin, "Acceleration and trapping of particles by radiation pressure," Phys. Rev. Lett. **24**, 156-159 (1970).
2. A. Ashkin, "Applications of Laser Radiation Pressure," Science **210**, 1081-1088 (1980).
3. K. Dholakia, P. Reece, and M. Gu, "Optical micromanipulation," Chem. Soc. Rev. **37**, 42-55 (2008).
4. A. Ashkin, J. M. Dziedzic, J. E. Bjorkholm, and S. Chu, "Observation of a single-beam gradient force optical trap for dielectric particles," Opt. Lett. **11**, 288-290 (1986).
5. D. G. Grier, "A revolution in optical manipulation," Nature **424**, 810-816 (2003).
6. A. Ashkin and J. M. Dziedzic, "Optical Trapping and Manipulation Of Viruses and Bacteria," Science **235**, 1517-1520 (1987).
7. A. Ashkin, J. M. Dziedzic, and T. Yamane, "Optical Trapping and Manipulation Of Single Cells Using Infrared-Laser Beams," Nature **330**, 769-771 (1987).
8. K. Svoboda and S. M. Block, "Biological applications of optical forces," Annu. Rev. Biophys. Biomol. Struct. **23**, 247-285 (1994).
9. M. Dienerowitz, M. Mazilu, and K. Dholakia, "Optical manipulation of nanoparticles: a review," J. Nanophot. **2**, 021875 (2008).
10. K. C. Neuman, T. Lionnet, and J.-F. Allemand, "Single-Molecule Micromanipulation Techniques," Annu. Rev. Mater. Res. **37,** 33-67 (2007).
11. S. Chu, "The manipulation of neutral particles," in *Nobel Lectures, Physics 1996-2000* (Ed. G. Ekspong, World Sc. Pub. Co., 2002), pp. 122-158.
12. H. Rubinsztein-Dunlop, T. A. Nieminen, M. E. J. Friese, and N. R. Heckenberg, "Optical trapping of absorbing particles," Adv. Quantum Chem. **30**, 469-492 (1998).
13. E. J. G. Peterman, F. Gittes, and C. F. Schmidt, "Laser-induced heating in optical traps," Biophys. J. **84**, 1308-1316 (2003).
14. D. McGloin, D. R. Burnham, M. D. Summers, D. Rudd, N. Dewara, and S. Anand, "Optical manipulation of airborne particles: techniques and applications," Faraday Discuss. **137**, 335-350 (2008).

#108707 - $15.00 USD Received 12 Mar 2009; revised 17 Mar 2009; accepted 18 Mar 2009; published 25 Mar 2009

15. E. J. Davis and G. Schweiger, *The Airborne Microparticle: Its Physics, Chemistry, Optics, and Transport Phenomena,* (Springer, 2002), pp. 780-785.
16. *Structured Light and its Applications: An Introduction to Phase-Structured Beams and Nanoscale Optical Forces*, ed. D. L. Andrews (Elsevier, Academic Press, 2008).
17. J. E. Curtis, B. A. Koss, and D. G. Grier, "Dynamic holographic optical tweezers," Opt. Commun. **207**, 169-175 (2002).
18. G. C. Spalding, J. Courtial, and R. Di Leonardo, "Holographic Optical Trapping," pp. 139-168 in Ref. [16].
19. K. Dholakia and P. J. Reece, "Near-field optical micromanipulation," pp. 107-138 in Ref. [16].
20. A. Ashkin and J. M. Dziedzic, "Optical Levitation by Radiation Pressure," Appl. Phys. Lett. **19**, 283-285 (1971).
21. R. Omori, T. Kobayashi, and A. Suzuki, "Observation of a single-beam gradient-force optical trap for dielectric particles in air," Opt. Lett. **22**, 816-818 (1997).
22. M. D. Summers, J. P. Reid, and D. McGloin, "Optical guiding of aerosol droplets," Opt. Express **14**, 6373-6380 (2006), http://www.opticsinfobase.org/oe/abstract.cfm?URI=oe-14-14-6373.
23. D. R. Burnham and D. McGloin, "Holographic optical trapping of aerosol droplets," Opt. Express **14**, 4175-4181 (2006), http://www.opticsinfobase.org/oe/abstract.cfm?URI=oe-14-9-4175.
24. G. Roosen and C. Imbert, "Optical levitation by means of two horizontal laser beams: a theoretical and experimental study," Phys. Lett. **59A**, 6 (1976).
25. N. Magome, M. I. Kohira, E. Hayata, S. Mukai, and K. Yoshikawa, "Optical Trapping of a Growing Water Droplet in Air," J. Phys. Chem. B **107**, 39883990 (2003).
26. M. Guillon, O. Moine, and B. Stout, "Longitudinal Optical Binding of High Optical Contrast Microdroplets in Air," Phys. Rev. Lett. **96**, 143902 (2006).
27. K. Taji, M. Tachikawa, and K. Nagashima, "Laser trapping of ice crystals," Appl. Phys. Lett. **88**, 141111 (2006).
28. A. Constable, J. Kim, J. Mervis, F. Zarinetchi, and M. Prentiss, "Demonstration of a fiber-optical light-force trap," Opt. Lett. **18**, 1867-1869 (1993).
29. R. G. Gauthier and A. Frangioudakis, "Optical levitation particle delivery system for a dual beam fiber optic trap," Appl. Opt. **39**, 26-33 (2000).
30. D. Rudd, C. Lopez-Mariscal, M. Summers, A. Shahvisi, J. C. Gutirrez-Vega, and D. McGloin, "Fiber based optical trapping of aerosols," Opt. Express **16**, 14550-14560 (2008), http://www.opticsinfobase.org/oe/abstract.cfm?URI=oe-16-19-14550.
31. D. M. Gherardi, A. E. Carruthers, T. Cižmár, E. M. Wright, and K. Dholakia, "A dual beam photonic crystal fiber trap for microscopic particles," Appl. Phys. Lett. **93**, 041110 (2008).
32. K. T. Gahagan and G. A. Swartzlander, Jr., "Optical vortex trapping of particles," Opt. Lett. **21**, 827-829 (1996).
33. M. P. MacDonald, L. Paterson, W. Sibbett, K. Dholakia, and P. E. Bryant, "Trapping and manipulation of low-index particles in a two-dimensional interferometric optical trap," Opt. Lett. **26** 863-865 (2001).
34. K. Svoboda and S. M. Block, "Optical trapping of metallic Rayleigh particles," Opt. Lett. **19**, 930-932 (1994).
35. H. Furukawa and I. Yamaguchi, "Optical trapping of metallic particles by a fixed Gaussian beam," Opt. Lett. **23**, 216-218 (1998).
36. K. Sasaki, M. Koshioka, H. Misawa, N. Kitamura, and H. Masuhara, "Optical trapping of a metal particle and a water droplet by a scanning laser beam," Appl. Phys. Lett. **60**, 807-809 (1992).
37. G. Roosen and C. Imbert, "The TEM_{01}^{*} mode laser beam - a powerful tool for optical levitation of various types of spheres," Opt. Commun. **26**, 432 (1978).
38. S. Sato, Y. Harada, and Y. Waseda, "Optical trapping of microscopic metal particles," Opt. Lett. **19**, 1807 (1994).
39. H. He, N. R. Heckenberg, and H. Rubinsztein-Dunlop, "Optical particle trapping with higher-order doughnut beams produced using high efficiency computer generated holograms," J. Mod. Opt. **42**, 217 (1995).
40. R. Dimova, H. Polaert and B. Pouligny, "Absorbing microspheres in water: laser radiation pressure and hydrodynamic forces," in *Scattering of Shaped Light Beams and Applications,* Eds. G. Gouesbet and G. Grehan (Research signpost, Trivandrum, INDE 2000) pp. 45-65.
41. J. F. Nye and M. V. Berry, "Dislocations in wave trains," Proc. R. Soc. London A **336**, 165 (1974).
42. M. S. Soskin and M. V. Vasnetsov, "Singular Optics," Prog. Opt. **42**, 219-276 (Ed. E. Wolf, Elsevier, 2001).
43. L. Allen, M. W. Beijersbergen, R. J. C. Spreeuw, and J. P. Woerdman, "Orbital angular momentum of light and the transformation of Laguerre-Gaussian laser modes," Phys. Rev. A **45**, 8185 - 8189 (1992).
44. *Optical Angular Momentum*, Eds. L. Allen, S. M. Barnett, and M. J. Padgett (Bristol, IOP Publ. 2003) pp. 314
45. M. E. J. Friese, J. Enger, H. Rubinsztein-Dunlop, and N. R. Heckenberg, "Optical angular-momentum transfer to trapped absorbing particles," Phys. Rev. A **54**, 1593 (1996).
46. M. E. J. Friese, T. A. Nieminen, N. R. Heckenberg, and H. Rubinsztein-Dunlop, "Optical torque controlled by elliptical polarization," Opt. Lett. **23**, 1-3 (1998).
47. N. B. Simpson, K. Dholakia, L. Allen, and M. J. Padgett, "Mechanical equivalence of spin and orbital angular momentum of light: an optical spanner," Opt. Lett. **22**, 52-54 (1997).
48. A. T. O'Neil, I. MacVicar, L. Allen, and M. J. Padgett, "Intrinsic and Extrinsic Nature of the Orbital Angular Momentum of a Light Beam," Phys. Rev. Lett. **88**, 053601 (2002).
49. H. He, M. E. Freise, N. R. Heckenberg, and H. Rubinsztein-Dunlop, "Direct observation of transfer of angular momentum to absorptive particles from a laser beam with a phase singularity," Phys. Rev. Lett. **75**, 826 (1995).

#108707 - $15.00 USD Received 12 Mar 2009; revised 17 Mar 2009; accepted 18 Mar 2009; published 25 Mar 2009

50. M. E. J. Friese, T. A. Nieminen, N. R. Heckenberg, and H. Rubinsztein-Dunlop, "Optical alignment and spinning of laser-trapped microscopic particles," Nature **394**, 348-350 (1998).
51. J. E. Curtis and D. G. Grier, "Structure of Optical Vortices," Phys. Rev. Lett. **90**, 133901 (2003).
52. V. Garcés-Chávez, D. McGloin, M. J. Padgett, W. Dultz, H. Schmitzer, and K. Dholakia, "Observation of the Transfer of the Local Angular Momentum Density of a Multiringed Light Beam to an Optically Trapped Particle," Phys. Rev. Lett. **91**, 093602 (2003).
53. K. Sakai and S. Noda, "Optical trapping of metal particles in doughnut-shaped beam emitted by photonic-crystal laser," Electron. Lett. **43**, 107-108 (2007).
54. F. Ehrenhaft, "On the physics of millionths of centimeters," Phys. Z. **18**, 352-368 (1917).
55. R. W. Lawson, "Photophoresis," Nature **103**, 514 (1919).
56. O. Preining, "Photophoresis," in *Aerosol Sciences* Ed. C. N. Davies (Academic Press, N. Y. 1966), pp. 111-135.
57. M. Lewittes, S. Arnold, and G. Oster, "Radiometric levitation of micron sized spheres," Appl. Phys. Lett. **40**, 455-457 (1982).
58. G. M. Hidy and J. R. Broc, "Photophoresis and the descent of particles into the lower stratosphere," J. Geophys. Res. **72**, 455 (1967).
59. G. T. Best and T. N. L. Patterson, "The capture of small absorbing particles by the solar radiation field," Planet. Space Sci. **9**, 801-809 (1962).
60. A. A. Cheremisin, Yu. V. Vassilyev, and H. Horvath, "Gravito-photophoresis and aerosol stratification in the atmosphere," J. Aerosol Sci. **36**, 1277-1299 (2005).
61. G. Wurm and O. Krauss, "Experiments on negative photophoresis and application to the atmosphere," Atm. Env. **42**, 2682-2690 (2008).
62. H. Rohatschek, "Levitation of stratospheric and mesospheric aerosols by gravito-photophoresis," J. Aerosol Sci. **27**, 467-475 (1996).
63. G. Wurm and O. Krauss, "Dust Eruptions by Photophoresis and Solid State Greenhouse Effects," Phys. Rev. Lett. **96**, 134301 (2006).
64. O. Krauss, G. Wurm, O. Mousis, J.-M. Petit, J. Horner, and Y. Alibert, "The photophoretic sweeping of dust in transient protoplanetary disks," Astron. Astrophys. **462**, 977 (2007).
65. O. Mousis, J.-M. Petit, G. Wurm, O. Krauss, Y. Alibert, and J. Horner, "Photophoresis as a source of hot minerals in comets," Astron. Astrophys. **466**, L9-L12 (2007).
66. J. Steinbach, J. Blum, and M. Krause, "Development of an optical trap for microparticle clouds in dilute gases," Eur. Phys. J. E **15**, 287-291 (2004).
67. E. G. Rawson and A. D. May, "Propulsion and angular stabilization of dust particles in a laser cavity," Appl. Phys. Lett. **8**, 93 (1966).
68. S. Arnold and M. Lewittes, "Size dependence of the photophoretic force," J. Appl. Phys. **53**, 5314 (1982).
69. A. B. Pluchino, "Photophoretic force on particles for low Knudsen number," Appl. Opt. **22**, 103 (1983).
70. H. Rohatschek, "Photophoretic levitation of carbonaceous aerosols," J. Aerosol Sci. **20**, 903-906 (1989).
71. J. Huisken and E. H. K. Stelzer, "Optical levitation of absorbing particles with a nominally Gaussian laser beam," Opt. Lett. **27**, 1223 (2002).
72. M. H. Rosen and C. Orr, "The photophoretic force," J. Colloid Sci. **19**, 50-60 (1964).
73. M. Pope, S. Arnold, and L. Rozenshtein, "Photophoretic spectroscopy," Chem. Phys. Lett. **62**, 589-591 (1979).
74. S. Arnold and Y. Amani, "Broadband photophoretic spectroscopy," Opt. Lett. **5**, 242-244 (1980).
75. A. B. Pluchino, "Radiometric levitation of spherical carbon aerosol particles using a Nd:YAG laser," Appl. Opt. **22**, 1861 (1983).
76. H. Rohatschek, "Direction, magnitude and causes of photophoretic forces," J. Aerosol Sci. **16**, 29-42 (1985).
77. H. Rohatschek, Acta phys. austriaca **10**, 267 (1956).
78. C. N. Alexeyev, M. A. Yavorsky, and V. G. Shvedov, "Angular momentum flux of counter-propagating paraxial beams," J. Opt. Soc. Am. B **25**, 643-646 (2008).
79. I. V. Basisty, M. S. Soskin, and M. V. Vasnetsov, "Optics of light beams with screw dislocations," Opt. Commun. **103**, 422-428 (1993).
80. E. G. Gamaly and A. V. Rode, "Nanostructures Created by Lasers," in *Encyclopedia of Nanoscience and Nanotechnology* **7**, 783-809 (Am. Sc. Pub., 2004).
81. B. Luther-Davies, V. Z. Kolev, M. J. Lederer, N. R. Madsen, A. V. Rode, J. Giesekus, K.-M. Du, and M. Duering, "Table-Top 50 W Laser System for Ultra-Fast Laser Ablation," Appl. Phys. A **79**, 1051-1055 (2004).
82. A. V. Rode, S. T. Hyde, E. G. Gamaly, R. G. Elliman, D. R. McKenzie, and S. Bulcock, "Structural analysis of a carbon foam formed by high pulse-rate laser ablation," Appl. Phys. A **69**, S755-S758 (1999).
83. A. V. Rode, E. G. Gamaly, and B. Luther-Davies, "Formation of cluster-assembled carbon nano-foam by high-repetition-rate laser ablation," Appl. Phys. A **70**, 135-144 (2000).
84. A. V. Rode, R. G. Elliman, E. G. Gamaly, A. I. Veinger, A. G. Christy, S. T. Hyde, and B. Luther-Davies, "Electronic and magnetic properties of carbon nanofoam produced by high-repetition-rate laser ablation, Appl. Surf. Sci. **197-198**, 644 (2002).
85. *CRC Handbook of Chemistry and Physics*, Ed. D. R. Lide, 88th ed. (CRC, Taylor & Francis Group, 2008).
86. W. A. de Heer, W. S. Bacsa, A. Chatelain, T. Gerfin, R. Humphrey-Baker, L. Forro, and D. Ugarte, "Aligned

#108707 - $15.00 USD Received 12 Mar 2009; revised 17 Mar 2009; accepted 18 Mar 2009; published 25 Mar 2009

Carbon Nanotube Films: Production and Optical and Electronic Properties," Science **268**, 845-847 (1995).
87. Z. P. Yang, L. Ci, J. A. Bur, S. Y. Lin, and P. M. Ajayan, "Experimental Observation of an Extremely Dark Material Made By a Low-Density Nanotube Array," Nano Lett. **8**, 446-451 (2008).
88. S. Beresnev, V. Chernyak, and G. Fomyagin, "Photophoresis of a spherical particle in rarefied gas," Phys. Fluids A **5**, 2043-2052 (1993).
89. L. D. Reed, "Low Knudsen number photophoresis," J. Aerosol Sci. **8**, 123-131 (1977).
90. J. C. Maxwell, "On Stresses in Rarified Gases Arising from Inequalities of Temperature," Phil Trans. R. Soc. London **170**, 231-256 (1879).
91. J. Plewa, E. Tanner, D. M. Mueth, and D. G. Grier, "Processing carbon nanotubes with holographic optical tweezers," Opt. Express **12**, 1978-1981 (2004), http://www.opticsinfobase.org/oe/abstract.cfm?URI=oe-12-9-1978.
92. C. Shi, Y. Zhang, C. Gu, L. Seballos, and J. Z. Zhang, "Manipulation and light-induced agglomeration of carbon nanotubes through optical trapping of attached silver nanoparticles," Nanotechnology **19**, 215304 (2008).

1. Introduction

When a photon is absorbed by a small particle its momentum contributes towards radiation pressure (RP) while its energy dissipates in heat. The RP forces [1, 2] are widely employed for micromanipulation [3] of particles with laser beams. The pioneering experiments of Ashkin [1] led to a broad range of applications of laser tweezers [4] spanning from trapping of colloidal particles [5] and living cells [6, 7, 8] to manipulation of nanoparticles [9], single molecules [10], and atoms [11]. However, the heating of absorbing particles by light [12, 13], in particular in gaseous media [14], may lead to much stronger thermal or *radiometric forces* [15], thus preventing direct use of RP forces and optical tweezers.

Optical tweezers. A major breakthrough by A. Ashkin [1] which allowed him to realize optical trapping of micron sized particles, "in liquids and gas," was to avoid radiometric effects by "suspending relatively transparent particles in relatively transparent media". Remarkably, Ref. [1] suggests three main designs for optical trapping experiment, namely: *a single-beam trap*, later developed [4] to utilize gradient force from a single strongly focused laser beam; *a dual beam trap*, allowing three-dimensional trapping based on the balance of forces between counter-propagating beams; and *a bottle beam*, subject of many recent publications. The excellent reviews cited above describe principles of operation of optical tweezers and probably the most advanced are the biological applications of a single-beam gradient optical trap for *transparent particles suspended in liquids*. Further developments of the techniques of shaping laser light [16], e.g. with spatial light modulators, lead to the so-called holographic optical tweezers [5, 17, 18] allowing simultaneous control over large number of particles. One of the recent developments in this area is the utilization of the evanescent fields of plasmonic and nano-structured surfaces to manipulate small particles [9, 19].

Trapping of *transparent particles in gases*, following original experiments on RP levitation in air and vacuum [1, 20], was developed later to levitate in air glass spheres [21] and liquid droplets [22, 23]. The dual beam horizontal optical trap has been used for trapping aerosol glass spheres [24], droplets of water [25] and oil [26], as well as ice crystals [27]. It has been implemented using optical fibers [28, 29, 30] and photonic crystal fibers [31]. Recent review on manipulation of transparent aerosol particles with RP can be found in Ref. [14].

Trapping of *absorbing particles in liquids* [12] is similar to the RP trapping of the so-called low-index transparent particles [32, 33] in the sense that both seek intensity minima, in contrast to transparent particles with refractive index higher than that of surrounding medium. For low-index particles the gradient force is repulsive, while for reflective (e.g. microscopic metallic) or absorbing particles the attractive gradient force is small in comparison with repulsive forces due to the direct transfer of the momentum from, correspondingly, scattered or absorbed photons. Note, however, that for subwavelength metal particles [34, 35] the attractive RP gradient force can again dominate other forces, including thermal, because of the excitation of surface creeping waves [35].

#108707 - $15.00 USD Received 12 Mar 2009; revised 17 Mar 2009; accepted 18 Mar 2009; published 25 Mar 2009

Other mechanisms have been suggested for trapping of micro-particles repelled by intensity maxima, namely a circularly scanning Gaussian beam [36] and the tube-like "doughnut" laser TEM_{01}^{*} mode [37] or Laguerre-Gaussian *vortex beam* [32, 38, 39, 40]. Optical vortex beam carries intensity zero at the origin of a ring-shaped transverse intensity profile because of a phase singularity and spatially twisted wave-front [41, 42], the later determines nonzero orbital angular momentum of photons [43, 44]. Particles absorbing photons also absorb their optical angular momentum: spin momentum from circularly polarized beams [45, 46, 47] and orbital momentum from vortex beams [47, 48, 49]. Both types of angular momentum lead to the effective mechanical torque and rotation of absorbing particles (note that transparent birefringent particles can be set into rotation by the circularly polarized beams only [50]). Different implementations of the vortex traps include use of azimuthally modulated vortices [51], multi-ring Bessel beams [52], or doughnut modes of photonic crystal lasers [53]. Recent review can be found in Ref. [16], in particular on trapping and rotating of particles with vortex beams.

The dissipation of absorbed photon energy leads to particle heating, but in liquids with high thermal conductivity the radiometric forces are significantly diminished so that the transfer of linear momentum from photons can be used for the RP trapping. However, if the laser power exceeds some maximal value, e.g. one milli Watt for magnetic particles in water [40], the radiometric effects may lead to boiling of surrounding liquid and bubble formation [12].

Trapping of ***absorbing particles in gases*** using optical tweezers is not possible because one of the radiometric forces, namely the *photophoretic force*, always dominates RP [1].

Photophoresis. Photophoresis (PP) was discovered by F. Ehrenhaft [54] in the course of investigating the elementary electric charge. PP is defined as the light induced motion of micron-sized particles in a gaseous medium; an overview of the early history of PP can be found in Refs. [55, 56]. PP occurs when the surface of a particle in a gaseous medium is nonuniformly heated by an incident light beam. Under such anisotropic heating, gas molecules rebound off the surface with different velocities creating an integrated force on the particle. For the case of a spherical particle, depending on whether the front or back surface is hotter, the particle will move away (positive PP) or toward the light source (negative PP) [15]. The rough comparison [57] of RP force, $F_{\rm rp} = P/c$, exerted by a beam with power P, and the PP force, $F_{\rm pp} = P/3v$, for particles with zero thermal conductivity [58], shows that for air at room temperature the later dominates by several orders of magnitude, $F_{\rm pp}/F_{\rm rp} = c/3v \simeq 6 \times 10^5$, here c is the speed of light and v is the gas molecular velocity.

The PP effect was shown to produce sufficient forces to balance out the gravitation and trap particles around sun [59], as well as in atmosphere [58, 60, 61] (the so-called gravito-PP [62], important for the solid state greenhouse effect [63]). It is an active area of research in planetary sciences [64, 65] and, in particular, the experiments at the International Space Station, aiming to simulate the aerosol behavior in Earth's atmosphere and the formation of planets in the early solar system, require optical traps for microparticle clouds in dilute gases [66].

In optics, since the early days of laser physics, the thermal forces acting on dust particles where directly observed in laser cavities, e.g. in lasers operating with doughnut mode TEM_{01}^{*}, or the optical vortex standing wave [67]. Different trajectories of particles were observed, including reversal of motion, but "no stationary trapping inside the beam". Similarly, instead of all-optical trapping, other works are dealing with levitation [57] of absorbing micro-particles utilizing a balance of the repulsive PP force by gravitation [68, 69, 70, 71]. In particular, the dependance of the levitating PP force on gas pressure was studied for aerosol agglomerates of carbon black particles [72], and the wavelength dependance of the PP force was used for the so-called PP-spectroscopy [73, 74].

The repulsive PP force for highly absorbing particles should push particles along the laser beam and out of the maximum. Thus the transverse trapping at the minimum of a mixture

#108707 - $15.00 USD Received 12 Mar 2009; revised 17 Mar 2009; accepted 18 Mar 2009; published 25 Mar 2009

of Gaussian and a doughnut vortex beams [57] is expected but the stable levitation was also observed with a nominally Gaussian beams [68, 69, 71]. The close examination of the non-paraxial focal region (Airy rings) suggested [75] that the particles were still trapped at intensity minima "being surrounded by regions of higher energy density and swirling energy flow". The complex pattern of the Poynting vector produces desirable trapping "potentials" for many micron-size spheres at once and the distortion from one particle can create trap for another [71].

The radiometric levitation was demonstrated several years prior [72] to the first experiments on RP trapping [1] but, to the best of our knowledge, the *stable PP trapping and manipulation of particles* was **not realized**. First probable reason is that until now the atmospheric and planetary sciences remain driving force for the research on PP and related laboratory experiments are designed specifically to compensate gravitation [61] or simulate light from the star (Sun) with a broad plane wave [76]. Second reason is that the time of thermalization across the particle is sufficient for its stochastic motion along complex trajectories, "such as simple or coiled helices, circles, oscillatory orbits, etc" [56], even with counter-propagating beams [77]. Nevertheless, as we show below, the PP force can be specifically tailored to achieve predictable, reliable, and easily controllable all-optical manipulation of absorbing aerosol particles.

Outline. We introduce a novel technique for PP trapping of clusters of absorbing carbon nanoparticles in air as well as demonstrate their stable positioning and dynamical guiding along the optical axis of two counter-propagating vortex beams. The experimental scheme is discussed in Sec. 2, together with observations of the transverse dynamics of trapped particles in real time. Section 3 describes nanoclusters collected from the PP trap, their optical and thermal properties, and provides an estimation of PP forces compared to much weaker RP and gravitation forces. The static and dynamic guiding of particles are discussed in Sec. 4 and the simultaneous trapping of a large number of particles is illustrated in Sec. 5. Concluding remarks and relevance of our results to other fields of optics and physics are summarized in Sec. 6.

2. Dual vortex beam trap

Our aim is to build an all-optical setup for trapping and manipulating absorbing aerosol particles seeking intensity minimum of illuminating light. The key step forward that we make here for realizing a fully three-dimensional trapping is the implementation of the horizontal dual beam scheme [1] but with co-rotating counter-propagating vortex beams [78]. The longitudinal on-axis confinement is achieved by a balance of the PP forces induced by two beams on the opposite sides of a particle, while the transverse confinement by the bright intensity ring compensates for gravity in the vertical plane.

2.1. Principle of operation

For a dual vortex trap shown schematically in Fig. 1, we take a particular care on the relative direction of rotation that is defined by the the topological charge of two optical vortices. For paraxial beams, the integer topological charge l determines the order of a phase dislocation of the complex electric field [41, 42], $E \sim \exp(il\varphi + ik_z z)$, here k_z is the wave-number and r and φ are, correspondingly, the polar radius and the azimuth in the transverse plain. Each time when the vortex beam is reflected, $k_z \to -k_z$, the rotation direction remains unchanged, $l \to l$, so that vortex effectively reverses its topological charge [78], defined with respect to the propagation direction z. In the schemes based on the Fabry-Perot interferometers with even number of reflectors, the counter-propagating vortex beams $E_1 \sim \exp(il_1\varphi + ik_z z)$ and $E_2 \sim \exp(-il_2\varphi - ik_z z)$ will have, therefore, opposite sense of rotation with topological charges $l_1 = l_2 = l$, and the interference intensity pattern $|E_1 + E_2|^2$ will be azimuthally modulated $\sim \cos(2l\varphi + 2k_z)$. The undesired intensity minima in the transverse intensity of composite trapping beam will allow particles to escape and should be avoided. Therefore, we employ a scheme where a single vor-

#108707 - $15.00 USD Received 12 Mar 2009; revised 17 Mar 2009; accepted 18 Mar 2009; published 25 Mar 2009

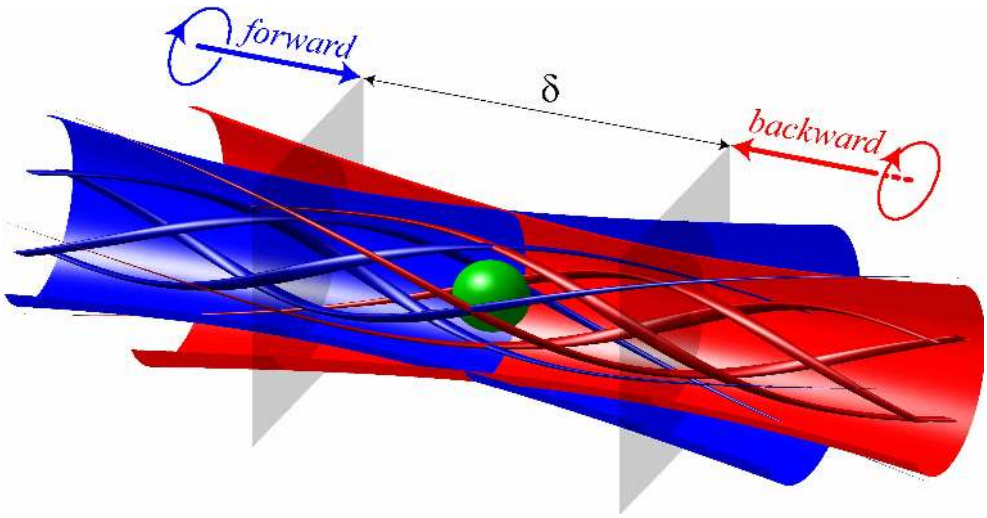

Fig. 1. Schematic of an optical trap with two counter-propagating and co-rotating vortex beams shown by surfaces at their tube-like intensity maxima. The focal (gray) planes of the froward (blue) and backward (red) beams are separated by the distance δ, for equal powers of two beams the trapping position is in the middle between two planes. Particle (green sphere) is subject to illumination from both sides, the geometry of the laser power flow (arrows) is shown with the stream-tubes, the varying width of tubes is proportional to the modulus of the Poynting vector.

tex beam is reflected odd number of times before allowing to counter-propagate itself, similar to a shearing interferometer. The sense of rotation of the initial and reflected beam coincide in this case, $l_2 = -l_1$, and azimuthal dependance $\exp(il_1\varphi)$ is factorized in the expression of the total field, thus the transverse intensity distribution remains radially symmetric, see Fig. 2(b). It is also noteworthy that such constructive interference effectively doubles the optical angular momentum [78], see the twisted power flow lines in Fig. 1.

2.2. *Experimental setup*

Our experimental setup is presented in Fig. 2. The linearly polarized Gaussian beam derived from a cw laser source (Verdi V5, Coherent Inc., wavelength $\lambda = 532$ nm) passes through diffraction fork-type hologram DH [39, 79] where it is transformed into a Laguerre-Gauss vortex beam with the topological charge $l = 1$; the transverse intensity pattern of the beam is shown in the inset (b). The beam diameter can be varied by a collimator based on two lenses, L1 and L2. The half-wave plate WP1 adjusts polarization of the input vortex beam so that it passes through the polarizing beam splitter BS1. The beam splitter serves as an injector of white light from the source WL to monitor the transverse dynamics of particles trapped in the trapping area C. The white light provides the background illumination for the images of the particles at the CCD2 camera after passing the notch filter NF which cuts off the laser radiation.

The interferometer consists of tree reflectors - a notch filter NF reflecting the laser beam, a mirror M, and a polarizing beam splitter cube BS2. The beam splitter BS2 divides the vortex beam into the forward-propagating beam (blue arrows) and the backward-propagating beam (red arrows). The forward beam passes through the lenses L3 and L4, reflects from the notch filter NF and mirror M, and exits the ring trough BS2. The backward beam reflects from BS2 and the mirrors M and NF, enters the trapping area in the opposite direction and goes through

#108707 - $15.00 USD Received 12 Mar 2009; revised 17 Mar 2009; accepted 18 Mar 2009; published 25 Mar 2009

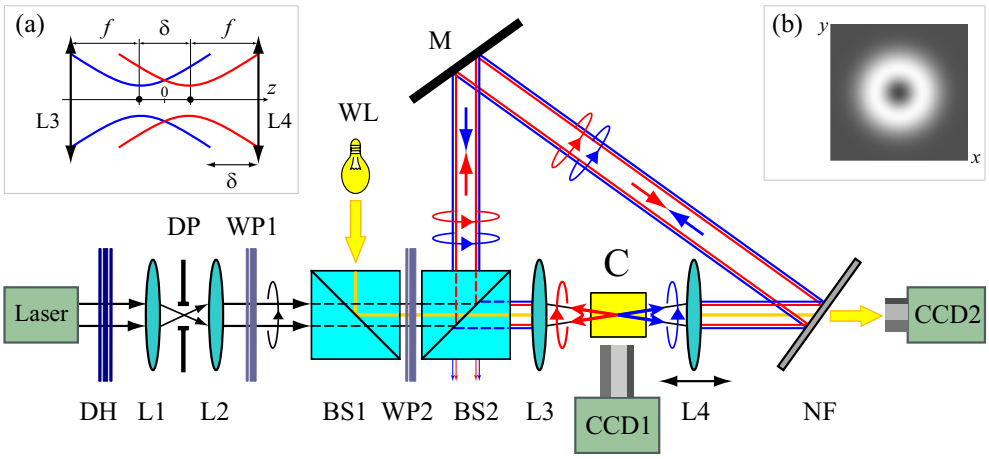

Fig. 2. Experimental setup. (a) Dual beam vortex trap with movable lens L4 adjusting the separation of focal planes δ. (b) The ring-like transverse intensity distribution of a Laguerre-Gauss vortex beam. Setup elements: DH – diffraction hologram, L – lenses, DP – diaphragm, WP – half-wave plates, BS – polarizing beam-splitters, WL – white light source, M – mirror, C – trapping region, NF – notch filter.

L4, L3, to exit the interferometer reflecting from BS2. The scheme is designed so that both beams have only a single round trip, thus preventing unwanted interference of the beams on the following paths. The interferometer is formed with the odd number of reflectors so that the axial symmetry of the intensity distribution is preserved for any polarization state of counter-propagating beams. The particle trapping volume C is formed between the lenses L3 and L4 and the distance δ between their focal planes can be varied by moving lens L4, see the inset (a) in Fig. 2. The imaging camera CCD1 collects the light scattered by the particles and monitors the behavior of the trapped particles in the longitudinal direction.

The half-wave plate WP2 allows gradually change the tilt angle θ of the polarization of the input optical vortex and thus to control the ratio $\varepsilon = P_f/P_b$ of the powers of forward P_f and backward P_b beams after the beam splitter BS2 with low extinction ratio 1:13. For full characterization of this important parameter we measured the powers of both beams inside the interferometer for two orthogonally polarized states, i.e., for $\theta = 0$ and $\theta = \pi/4$. Applying Malus' law we derive the expression

$$\varepsilon(\theta) = \frac{1}{\gamma}\,\frac{\alpha\cos^2 2\theta + \beta\sin^2 2\theta}{1-\alpha\cos^2 2\theta - \beta\sin^2 2\theta}, \quad 0.093 \le \varepsilon \le 15.623, \tag{1}$$

here $\alpha = 0.928$ and $\beta = 0.071$ are the coefficients of transmission through BS2 for two orthogonal linear polarizations and $\gamma = 0.825$ is the transmission coefficient through the long arm of the interferometer taking into account loses of the backward beam on the mirror M and notch filter NF. The total working power $P = P_f + P_b$ inside the interferometer is less than the power P_{in} passing from the laser onto the beam-splitter cube BS1 because of loses $\gamma < 1$. It can be calculated as $P/P_{\text{in}} = \gamma + (1-\gamma)(\alpha\cos^2 2\theta + \beta\sin^2 2\theta)$ and it varies slightly with θ, $0.837 \le P/P_{\text{in}} \le 0.987$.

2.3. *Transverse dynamics of trapped particles*

When a small amount of particles is released in air in the vicinity of the trapping region, we observe fascinating scattering of many particles drawn towards the trap and competing for a

#108707 - $15.00 USD Received 12 Mar 2009; revised 17 Mar 2009; accepted 18 Mar 2009; published 25 Mar 2009

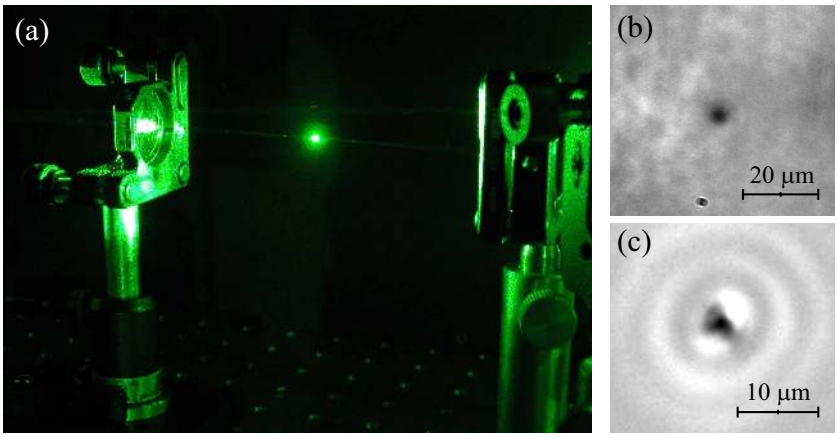

Fig. 3. Photophoretic trap. (a) The side view of the setup with a particle trapped in air. A halo of the scattered light makes particle visible to a naked eye. (b, c) The shade cast by a trapped particle as seen on the optical axis on white-light background in (b) (Media 1) and with superimposed vortex beam in (c)(Media 2).

stable position. The nanoclusters scatter sufficient amount of light to be visible by a naked eye, as is seen in Fig. 3(a), while the temperature of the particle in the trap is well below the activation temperature of 300°C for graphite oxidation. Once being captured, a particle remains stationary for many hours and the PP trapping is sufficiently robust to trap particles even when the operating power is reduced below one milli Watt. The PP trap in Fig. 3(a) was formed using lenses L3 and L4 with focal distance $f = 60$ mm, operating the laser power $P = (1-10)$ mW, and the vortex beam radius (waist) $w = 8.4\,\mu$m.

We use a white-light source to monitor the transverse dynamics of trapped particles on the CCD2 camera (see Fig. 2). Figure 3(b) and (Media 1) shows the dynamics of a shade cast by a trapped particle on the white-light background with the notch filter NF blocking the laser beam. In this experiment, we use the lenses L3 and L4 with focal distances $f = 35$ mm, the vortex ring radius $w = 4.1\,\mu$m, and operating power $P = 1.44$ mW. In Fig. 3(b) and (Media 2) we modify the conditions of the trapping by decreasing gradually the operating power in real time, from $P = 30.6$ mW in the beginning, when the laser light passing through the notch filter NF is sufficient to visualize the vortex profile, as in Fig. 3(c), to $P = 0.3$ mW, when only a white-light background remains visible in (Media 2). Stability of the trapping in the transverse cross-section can be estimated from the fluctuations of the particle position in (Media 1) and (Media 2); a typical value is within $\pm 2\,\mu$m and it is improving (decreasing) with the increase of the laser power P.

3. Carbon nanoclusters and photophoretic force

3.1. Properties of carbon nanoclusters

For the PP-based trapping in air we use "black" clusters of agglomerated carbon nanoparticles [80] produced with high repetition-rate laser ablation technique [81]. To produce samples for this study, the graphite targets were ablated in a vacuum chamber pumped to a base pressure of 10^{-3} Torr and then filled with high-purity (99.995%) argon gas. Figure 4(a) shows a TEM image of individual nanoparticles deposited on a holey carbon TEM grid located near the ablated graphite target. The average size of individual nanoparticles range from 4 nm to 8 nm depending on the buffer gas pressure, as seen in the inset in (a). The nanoparticles agglomerate

#108707 - $15.00 USD Received 12 Mar 2009; revised 17 Mar 2009; accepted 18 Mar 2009; published 25 Mar 2009

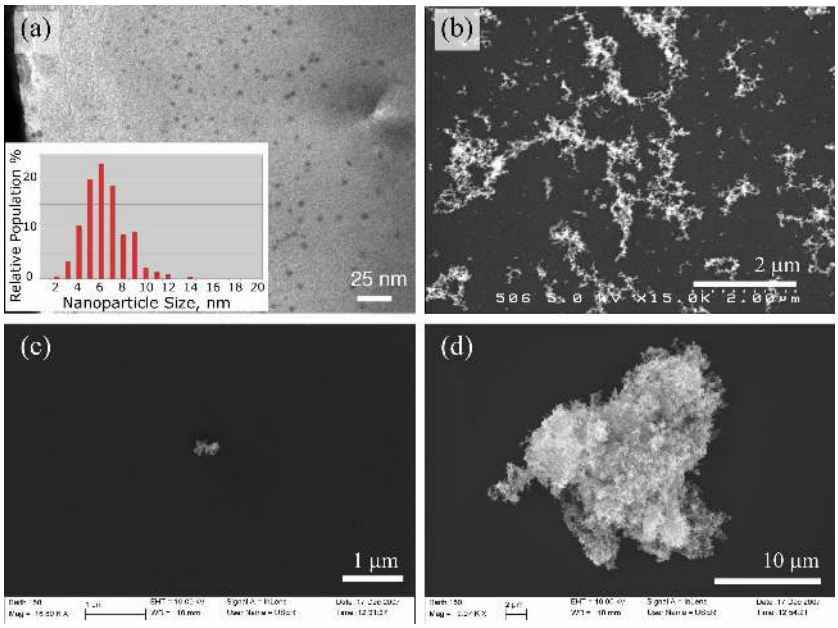

Fig. 4. Electron micrographs of carbon nanoclusters produced by laser ablation and collected from an optical trap. (a) TEM micrograph of single nanoparticles deposited on a holey carbon TEM grid in the laser ablation chamber. The inset shows the nanoparticle size distribution with the maximum at 6 nm; (b) SEM image of nanoparticle aggregates used in the trapping experiments; (c,d) SEM images of carbon nanoclusters collected from the PP trap. The vortex beam radius in these experiments was $w = 8.4\,\mu$m.

into the so-called nanofoam due to a diffusion-limited aggregation process, see the SEM image in Fig. 4(b); fragmented nanofoam is used in our experiments as a source of aerosol particles. Carbon nanofoam is synthesized [82, 83, 84] using 40 W frequency doubled Nd:YVO_4 laser generating 12 ps pulses at wavelength $\lambda = 532$ nm with repetition rate 1.5 MHz. The laser intensity on a target surface is $\sim 10^{12}$ W/cm^2 with the corresponding fluence of up to 20 J cm^{-2}. The density of individual nanoparticles determined by the electron energy loss technique [83] is in the range $\rho_g = (1.65-1.90)$ g cm^{-3}, while the bulk density of the carbon nanofoam is varied in the range $\rho_f = (2-20)$ mg cm^{-3}, depending on the argon pressure [84].

One of the key parameters for the radiometric effects is the thermal conductivity of particles. To estimate it for carbon nanoclusters we assume that nanofoam consists of a mixture of graphite nanospheres and air with a volume filling fraction $\eta = (\rho_f - \rho_a)/(\rho_c - \rho_a)$. Taking the average density of the nanofoam $\rho_f = 10$ mg cm^{-3} [83], of air $\rho_a = 1.29$ mg cm^{-3}, and of a nanoparticle $\rho_g = 1.8$ g cm^{-3}, we obtain $\eta = 4.84 \times 10^{-3}$. Due to such low density we find, using the linearized Maxwell formula, $k_f \simeq k_a(1+3\eta)$, that the nanofoam thermal conductivity, $k_f = 0.0266$ W m^{-1} K^{-1}, is mainly determined by that of air, $k_a = 0.0262$ W m^{-1} K^{-1} [85].

The record low-bulk density and low-thermal conductivity makes agglomerates of carbon nanoparticles a nearly ideal substance for the experiments with the PP trapping. Moreover, the absorption of nanostructured carbon is high while reflectivity is extremely low [86, 87] which makes such particles approach the properties of a black body. The SEM images of nanoclusters collected on silicon wafers directly from the trap are presented in Fig. 4(c,d). Among many collected particles of different shapes and sizes, in (c) we show one of the smallest, with the linear size of the order of 100 nm, and in (d), one of the largest with the characteristic size of

#108707 - $15.00 USD Received 12 Mar 2009; revised 17 Mar 2009; accepted 18 Mar 2009; published 25 Mar 2009

$10\,\mu$m; both samples have been collected from the same trap with the vortex radius $8.4\,\mu$m.

3.2. Evaluation of optical forces in the trap

Calculation of the PP force is a complicated task, it involves solving the electrodynamic and gas-kinetic equations self-consistently, taking into account thermophysical, optical, and accommodation properties of an aerosol particle [15, 88]. The important parameter [88, 89] that distinguishes two different physical situations is a ratio of the mean free path of the gas molecule l to the characteristic size of the particle a or the Knudsen number $K = l/a$. In the so-called free-molecule regime, for $K > 1$, the gas kinetic theory applies [58]. For low values of the Knudsen number $K < 1$ the PP force is a result of the Maxwellian "thermal creep" of the gas molecules along the temperature gradient on the particle surface [90], and the gas is modeled as a continuous fluid medium with the boundary slip flow conditions [89].

The theory of the PP force has been developed for a spherical particle illuminated by a plane wave. Therefore, we model a particle by a sphere with thermal and optical properties of the nanofoam, typical radius $a = 1\,\mu$m, and illuminated by a plane wave with characteristic intensity $I = 1$ kW cm^{-2}. First, we estimate the RP force due to the absorption of the photon linear momentum, $F_{\rm rp} = P_{\rm abs}/c = 4 \times 10^{-15}$ N, here $P_{\rm abs} = 4\pi I a^3/3l_f = 1.2 \times 10^{-6}$ W is the power absorbed by a particle. The absorption length $l_f = 35\,\mu$m is obtained from optical transmission measurements of the carbon nanofoam films with thicknesses varying in the range $(70 - 120)\,\mu$m. The absorbtion efficiency of the particle, i.e. the ratio $\xi = P_{\rm abs}/P_{\rm in}$ of the absorbed to the incoming power $P_{\rm in} = \pi a^2 I$, is of the order of a few percent, $\xi = 4a/3l_f = 0.038$.

For evaluation of the PP force we apply the limit of total accommodation and low Knudsen number, $K = l/a = 0.065$, here $l = 65$ nm is the mean-free path of air molecules. The expression for the PP force is given by (see, e.g., formula (34) in Ref. [88])

$$F_{\rm pp} = -J_1 \frac{9\pi\mu_a^2 a I_0}{2\rho_a T(k_f + 2k_a)},$$

here the air viscosity $\mu_a = 1.73 \times 10^{-5}$ Ns/m^2 at room temperature. The important parameter which defines the sign and the magnitude of the PP force is an asymmetry factor J_1; for black body particles $J_1 = -0.5$. Although the nanofoam skin-depth $l_f = 35\,\mu$m is larger than typical nanocluster dimension, the thermal conductivity k_f is very low (see above), thus we can assume that the temperature changes on the particle surface are determined by the illuminating intensity only, similar to the black body particles [87]. The factor J_1, however, also takes into account corresponding absorption efficiency ξ, thus we adopt the following value: $J_1 = -\xi/2 = -2a/3l_f$. In these assumptions the $F_{\rm pp}$ force dominates RP force $F_{\rm rp}$ by four orders of magnitude, $F_{\rm pp} = 3 \times 10^{-11}$ N. For comparison, the gravitational force is $F_g = mg = 4.1 \times 10^{-16}$ N, here $g = 9.81$ m s^{-2} is the standard gravity and the particle mass $m = 4\pi\rho_f a^3/3 = 4.2 \times 10^{-14}$ g.

The magnitude and direction of the PP force depend on the size of the individual particle as well as the surface properties. First, the surface temperature depends not only on the distribution of heat sources (absorption centers) within the particle, but also on a complex shape which enters into the boundary conditions of the heat conduction. Second is that an additional surface creep effect may play a role if the accommodation of the gas molecules on particle surface varies; the direction of the flow is from the side of higher to the side of lower accommodation coefficient. Both these effects might only increase PP force [70, 76]. Therefore, our estimation of the PP force above is sufficiently conservative.

#108707 - $15.00 USD Received 12 Mar 2009; revised 17 Mar 2009; accepted 18 Mar 2009; published 25 Mar 2009

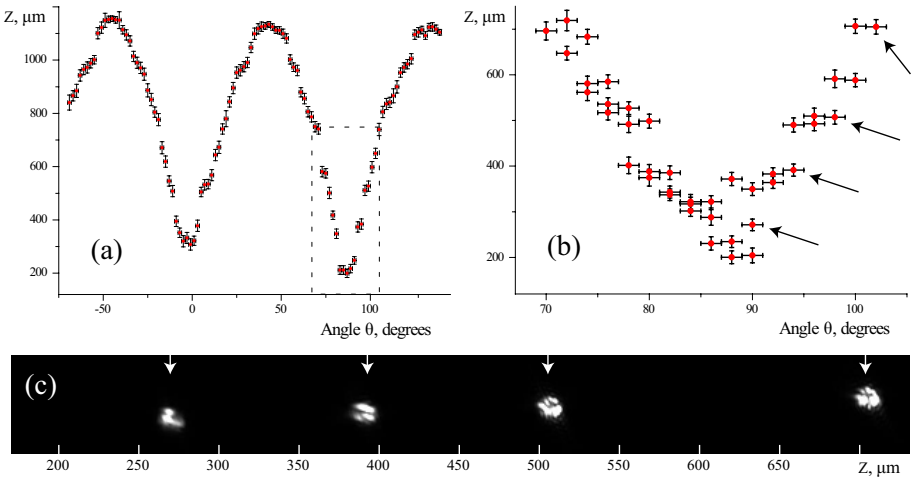

Fig. 5. Static guiding of particles in air. The position Z of a trapped particle measured as a function of the polarizer angle θ in (a) and with higher magnification in (b). Vertical bars measure the spot size of the recorded particle images such as those superimposed in (c)(Media 3); corresponding data points are marked in (b) with arrows.

4. Optical manipulation experiments

Optical guiding of the trapped particles along an optical axis is achieved by varying the tilt angle θ of the half-wave plate (see Sec. 2), and thus changing the power ratio $\varepsilon(\theta) = P_f/P_b$ of the forward (P_f) and backward (P_b) vortex components. Imbalance of the powers illuminating a particle from both the sides shifts the trapping position towards the beam with the lower power. Below we demonstrate *static guiding*, i.e. the ability to pinpoint trapped micro-particle in a stable position anywhere within one-millimeter distance on the optical axis. In addition, we demonstrate *dynamic guiding* of trapped particles by periodically bouncing them forward and backward in real time between two limiting positions separated by more than two millimeters.

4.1. Static guiding

The images of radiation scattered by trapped particles in the direction perpendicular to the optical axis are presented in Fig. 5. We realize a static trapping for each tilt θ changed by the steps of 2°. The focal planes are separated by $\delta = 2$ mm and we could stably pinpoint the particle anywhere on the axis of the beam within the distance of about 1 mm, see Fig. 5(a). We also notice that the particle does not return to the same position for a given θ. In the similar experiments but with the maximum magnification of our imaging system [Figs. 5(b,c)] the half-wave plate is turned three times about one of the extrema points, indicated in Fig. 5(a) by a dashed rectangle. The deviation of the trapping position Z versus θ reaches the values up to $200\,\mu$m, greatly exceeding the position uncertainty for a stationary particle. The later is determined as the recorded spot size $\sim 10-20\,\mu$m in Fig. 5(c) and indicated by vertical bars in Figs. 5(a,b). Although the trapped particle undergoes Brownian motion, we rule out instability of trapping because we never observe a trapped particle to change its position spontaneously. The most plausible explanation for the observed hysteresis-type behavior is the presence of additional multiple traps produced by a rather large distortion in the shape of the vortex beams and misalignment of their axes.

Nevertheless, it is always possible to position the particle, by appropriately adjusting $\varepsilon(\theta)$, with a precision limited only by the resolution of our imaging system. In the stationary position

#108707 - $15.00 USD Received 12 Mar 2009; revised 17 Mar 2009; accepted 18 Mar 2009; published 25 Mar 2009

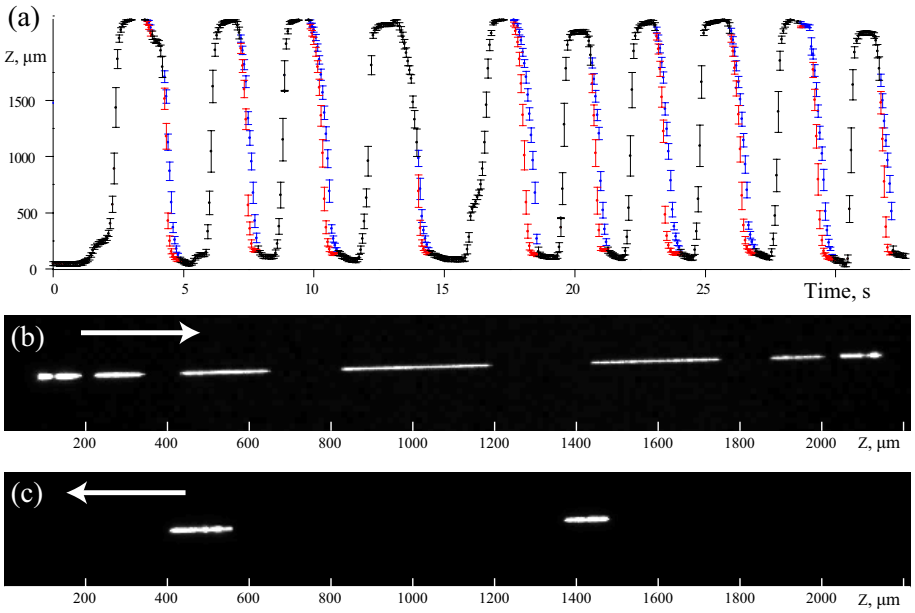

Fig. 6. Dynamic guiding of particles in air (Media 4). Positions of two particles simultaneously bouncing between two extrema points of the trap vs. time are shown in (a); black bars correspond to the on-the-fly tracks overlapping for both particles, such as nine consecutive tracks superimposed in (b). Blue and red bars in (a) measure two tracks of separated particles, such as those shown in the snapshot of (c) at $t = 23$ s. Arrows in (b) and (c) indicate the directions of propagation.

the typical real time dynamics of the light scattered off-axis is that of a speckle field, it is presented in (Media 3) as seen at CCD1 camera, and it corresponds to the images in Fig. 5(c); each image is taken from a sequence similar to that shown in the video but at different axial locations of the trap. In this experiment, the focal distances of the lenses L1 and L2, $f = 60$ mm, the vortex ring radius 8.4 μm, and power $P_{in} = 1.6$ mW.

4.2. *Dynamic guiding*

To test the dynamic stability of the PP trapping, we perform hand-on experiments on the continuous movement of particles recording on-the-fly tracks with exposition 40 ms. A half-wave plate is rotated changing $\varepsilon(\theta)$ periodically so that the particles are bouncing back and forward many times over the distance exceeding 2 mm and reaching the velocities up to 1 cm/s (here the inter-focal distance is $\delta = 7.4$ mm and other parameters as for static guiding above). The results are presented in Figs. 6 (Media 4); we notice that the particle dynamics is somewhat similar to a ping-pong ball. The position Z versus real time in (a) is determined as the length of the tracks (vertical bars) recorded with finite exposition time. In this particular experiment we have two particles trapped simultaneously but they are visibly separated only when moving in one direction, from the right to left, as shown in the snapshot in (c). At any moment of this experiment the rotation could be stopped and the particles stop and become indistinguishable. Similarly, it is impossible to distinguish two particles when their tracks overlap on the flight from the left to right in (b). The asymmetry between two-way motions indicates that the recorded particles have different sizes (masses) but retain their relative positions on the axis, namely smaller and lighter particle, on the left, and larger and heavier particle, on the right. The

#108707 - $15.00 USD Received 12 Mar 2009; revised 17 Mar 2009; accepted 18 Mar 2009; published 25 Mar 2009

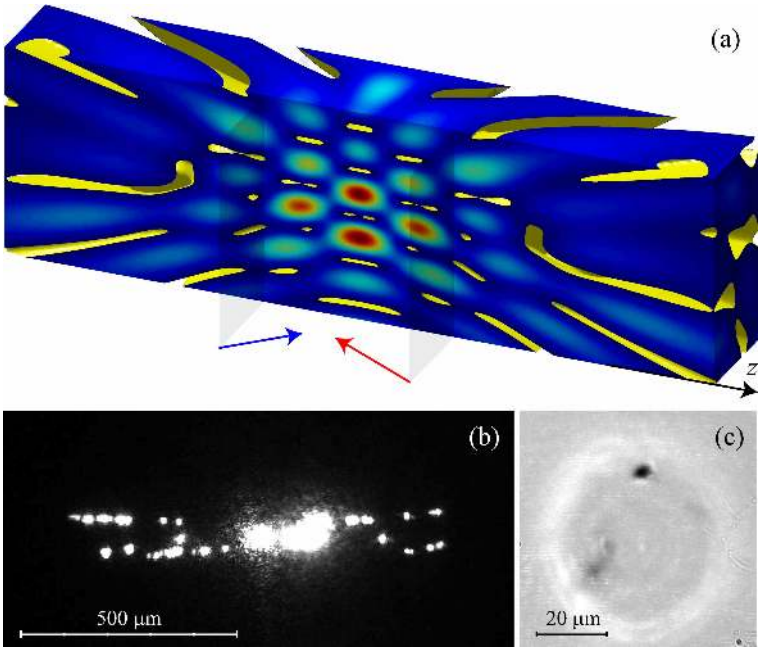

Fig. 7. Multiple PP trap with tilted beams. (a) Volume plot of the longitudinal cut through the total intensity calculated for two counter-propagating Laguerre-Gaussian beams LG_{12} tilted in the vertical direction by 0.02 rad. The yellow surfaces cut out the regions of small intensity where particles can be trapped. (b)(Media 5) The side view and (c)(Media 6) the front view of several particles simultaneously trapped with tilted beams.

later would accelerate slower and delay on the flight to the left.

5. Multiple particle trapping

The observations above suggest that the PP trap can be employed for simultaneous trapping of many particles. To elucidate this possibility we consider more complex multi-ring vortices created by the Laguerre-Gaussian beams LG_{ln}, where the integer index n indicates, in addition to the beam topological charge l, the number of radial nodes (dark rings) in the transverse intensity distribution. Calculating the total intensity of the superposition of such co-rotating counter-propagating vortices we also assume a small relative tilt of their optical axes. This tilt results in a complex light pattern with multiple minima shown in Fig. 7(a). Experimental results are presented in Figs. 7(b,c); the parameters of the setup and operating power as the same as in (Media 1). In contrast to a single trap, the particles interact strongly in a multiple trap as seen in (Media 5); the dynamics of particles suggests an analogy with a "spider-web" for flying particles. Figure 7(c) and (Media 6) demonstrate several particles trapped simultaneously as seen on-axis CCD2 camera, similar to (Media 1) and (Media 2). During the playback, the focal plane of the imaging lens is shifted along the optical axis so that it effectively scans the multiple traps and allows visualizing several particles.

We estimate that the number of trapped particles seen in Fig. 7 is about one hundred. Combining several such beams or employing holographic technique [3] it is possible to create a "web" of vortex traps in a significant volume trapping a large number of particles [91].

#108707 - $15.00 USD Received 12 Mar 2009; revised 17 Mar 2009; accepted 18 Mar 2009; published 25 Mar 2009

6. Conclusions

In summary, our proof-of-principle experiments utilize the PP force for trapping and transporting absorbing particles in gases. The access to optical forces exceeding the RP force by several orders of magnitude opens novel perspectives for reliable manipulation of particles. Our projections show that an up-scaling of an optical beam size will allow larger particles to be trapped and transported over longer distances, keeping trapping powers as low as few milli-Watts. Alteration of physical properties of airborne particles is minimal in our trap because only a small fraction of the operating power is absorbed at the vortex core where the intensity vanishes. Therefore, the particles agglomerated and collected in the non-contact and remote trap can be further investigated in terms of their chemical activity, composition, and purity as compared to a bulk. The ability of remote and non-contact volume localization of air-born nanoclusters with optical vortices may find wide applications in engineering and control equipment for manufacturing and micro-assembly processes [92]. Our approach and results can be important for other fields, such as interstellar dusty plasmas and atmospheric physics.

Acknowledgments

The authors acknowledge a support from the National Health and Medical Research Council (NHMRC) of Australia and the Australian Research Council (ARC).

#108707 - $15.00 USD Received 12 Mar 2009; revised 17 Mar 2009; accepted 18 Mar 2009; published 25 Mar 2009